



HAL
open science

The water vapour self- and foreign-continua in the 1.6 μm and 2.3 μm windows by CRDS at room temperature

S. Vasilchenko, A. Campargue, S. Kassi, D. Mondelain

► **To cite this version:**

S. Vasilchenko, A. Campargue, S. Kassi, D. Mondelain. The water vapour self- and foreign-continua in the 1.6 μm and 2.3 μm windows by CRDS at room temperature. *Journal of Quantitative Spectroscopy and Radiative Transfer*, 2019, 227, pp.230-238. 10.1016/j.jqsrt.2019.02.016 . hal-02079821

HAL Id: hal-02079821

<https://hal.science/hal-02079821>

Submitted on 22 Oct 2021

HAL is a multi-disciplinary open access archive for the deposit and dissemination of scientific research documents, whether they are published or not. The documents may come from teaching and research institutions in France or abroad, or from public or private research centers.

L'archive ouverte pluridisciplinaire **HAL**, est destinée au dépôt et à la diffusion de documents scientifiques de niveau recherche, publiés ou non, émanant des établissements d'enseignement et de recherche français ou étrangers, des laboratoires publics ou privés.



Distributed under a Creative Commons Attribution - NonCommercial 4.0 International License

Abstract

50
51
52
53
54
55
56
57
58
59
60
61
62
63
64
65
66
67
68
69
70
71
72
73

New measurements of the water vapour continuum in the 1.6 μm and 2.3 μm windows are obtained at room temperature using highly stable and sensitive cavity ring down (CRD) spectrometers.

In the 1.6 μm window, self-continuum cross-sections, C_S , are derived for 30 selected spectral points between 5700 and 6850 cm^{-1} using pressure ramps (up to 15 Torr) of pure water vapour. Purely quadratic pressure dependence is obtained for each measurement point. Compared to our previous dataset (Mondelain *et al.*, J. Geophys. Res. Atmos. (2014) 119, 2169–8996), the retrieved C_S values are more accurate and show a general agreement. The spectral coverage is extended both on the high and low frequency edges of the 1.6 μm window. In addition, new C_S values are derived in the 5120-5137 cm^{-1} interval extending to higher energy the coverage of the 2.3 μm window. The measurements near 5700 cm^{-1} and 5130 cm^{-1} are found lower than the MT_CKD values by a factor of about 2 and 1.5, respectively.

Foreign-continuum cross-sections, C_F , are newly obtained in the 2.3 μm window from CRDS spectra of moist air in flow regime. Spectra were recorded for different water vapour partial pressures while maintaining the total pressure constant in the high finesse CRDS cavity. After subtraction of the monomer and self-continuum contributions, C_F values were derived from the linear variation of the foreign-continuum absorption with the water vapour partial pressure. C_F values determined at four spectral points between 4430 and 5000 cm^{-1} are larger by up a factor of five than the corresponding MT_CKD values. Considering these CRDS data at room temperature and literature values at 400 K the temperature dependence of the foreign-continuum is confirmed to be weak.

74 **1. Introduction**

75 Absorption of water vapour plays a key role in the radiative budget of the Earth's atmosphere
76 [1]. This absorption corresponds to the sum of the narrow rovibrational absorption lines,
77 hereafter named "local line monomer", with the broadband water vapour continuum, slowly
78 varying in frequency. This latter contribution has its largest impact in transparency windows
79 (or regions of weak monomer absorption) in contrast to the regions corresponding to the water
80 vapour vibrational bands where the monomer contribution largely dominates. In a mixture of
81 water vapour in air, like the Earth's atmosphere, two contributions of the continuum are
82 present: (i) the self-continuum due to interactions between two water molecules and (ii) the
83 foreign-continuum arising from interactions between water molecules and molecular oxygen
84 and nitrogen. Despite decades of debates [2], the origin of the water continuum is unclear with
85 different processes suggested to contribute: far wings of the rovibrational lines, water dimers
86 (stable and metastable) and collision-induced absorption (CIA) [3].

87 The semi-empirical MT_CKD model (Mlawer-Tobin_Clough-Kneizys-Davies) [4,5] is the
88 usual pragmatic way to take into account the continuum absorption contribution of the water
89 vapour in atmospheric radiative transfer codes. This model assumes an empirical line profile
90 applied to all the water monomer transitions, with intermediate and far line wings fitted to
91 reproduce a selection of laboratory and atmospheric data. The MT_CKD model also includes
92 an additional term called "weak interaction" term.

93 During the two last decades large efforts have been done to complete previous experimental
94 data [6,7,8] and to better characterize the water vapour continuum, particularly in the infrared
95 windows. Several laboratory studies were dedicated to the measurement of the self-continuum
96 cross-sections using Fourier transform spectroscopy (FTS) [9,10,11,12] and cavity-enhanced
97 absorption spectroscopy (CEAS) including cavity ring down spectroscopy (CRDS) and
98 optical feedback CEAS (OFCEAS) [13,14,15,16]. The FTS room temperature self-continuum
99 cross-section values, in relatively good agreement to each other, were found largely higher
100 than the MT_CKD_2.5 cross-sections in the centre of the 2.1 and 1.6 μm windows by factors
101 greater than 20 [10,11,12] and 160 [11,12], respectively. On the other hand, as a result of their
102 inherent higher sensitivity and high baseline stability, CEAS studies of our group provided
103 datasets with reduced uncertainties. They were found in a much better agreement with the
104 MT_CKD model [16]. Note that our CRDS and OFCEAS measurements [14,15,16] rely on
105 the careful checking of the quadratic pressure dependence of the continuum absorption which
106 provides a key criterion to ensure the gas phase origin of the spectrum baseline variation. This
107 is not the case for the FTS results at room temperature which relied on single pressure spectra

108 measurements in the windows. The latest version (3.2) of the MT_CKD self-continuum was
109 constrained to the CEAS cross-sections in the 4.0, 2.1, 1.6 and 1.25 μm windows [17].

110 In fact, a pure quadratic pressure dependence was achieved in all our CRDS and OFCEAS
111 studies of the water vapour self-continuum except in the 1.6 μm window where the weak
112 continuum signal was found to include not only a pressure squared term but also a linear term
113 in P_{H_2O} [18,19]. This linear term was tentatively interpreted as due to the adsorption of the
114 water molecules on the high reflective mirrors of the CRDS cell. In this situation, the
115 accuracy of our C_s values in the 1.6 μm window was questioned [20]. This is the reason why
116 in the present contribution, we reconsider the 1.6 μm window where measurements are
117 particularly demanding as a result of the weakness of the continuum in this window. In
118 addition, the spectral coverage of this window will be extended on its two edges.

119 The foreign-continuum of water vapor in air is a major source of uncertainty to be constrained
120 in Earth atmospheric models because, under standard conditions, it might account for a
121 significant fraction of the absorbed incoming solar flux [21,22]. In the laboratory, the foreign-
122 continuum cross-sections are derived from spectra recorded with moist nitrogen (or air) which
123 include both a foreign- and a self-contribution. As a result, the obtained foreign-continuum
124 cross-sections, C_F , are directly impacted by the self-continuum cross-sections values, derived
125 separately with pure water vapor samples. The review included in [23], indicates that only a
126 few experimental studies of the water foreign-continuum are available. The reference [24]
127 describing CRDS measurements at 944 cm^{-1} should be added to the seven references listed in
128 Table 6 of Ref. [23]. The FTS results obtained at NIST [25,26,27] and by CRDS in the 2.1
129 μm window [21] match and have led to a significant increase of the MT_CKD foreign-
130 continuum model in the transparency windows. Note that, in the limit of the reported error
131 bars, the foreign-continuum has been found to be mostly temperature independent in the
132 broad-band CAVIAR FTS measurements between 350 and 430 K. Similar weak temperature
133 dependence results were reported in the infrared in the 296-363 K range [25,26] and in the
134 260-360 K range near 183 GHz [28].

135 In the following, we will present the experimental determination of the foreign-continuum by
136 CRDS at room temperature for four new spectral points of the 2.3 μm window and the
137 production of an extended dataset for the self-continuum cross-sections in the 1.6 μm
138 window.

139 The rest of the paper is organized as follows. In the next section, the experimental setups used
140 for the self- and foreign-continua measurements are detailed. The data analysis and the cross-

141 sections retrievals are presented in Part 3 and 4 for the self-continuum in the 1.6 μm window
 142 and for the measurements in the 2.3 μm window, respectively. These two parts include a
 143 comparison to experimental data available in the literature and to the MT_CKD model, and a
 144 detailed analysis of the error budget.

145 **Table 1.** Spectral points selected for the present continua measurements by CRDS in the 2.3 and 1.6
 146 μm windows and corresponding self- and foreign-continuum cross-sections values. TW (This work)
 147 marks the newly derived values.
 148

Window Approx. center	Measurement points (cm^{-1})	C_S ($\text{cm}^2 \text{ molecule}^{-1} \text{ atm}^{-1}$)	C_F ($\text{cm}^2 \text{ molecule}^{-1} \text{ atm}^{-1}$)
4700 cm^{-1} (2.1 μm)	4432.6	1.19(6) $\times 10^{-23}$ [15]	1.26(5) $\times 10^{-25}$ (TW)
	4436.3	1.18(6) $\times 10^{-23}$ [15]	1.15(5) $\times 10^{-25}$ (TW)
	4522.0	9.33(25) $\times 10^{-24}$ [14]	8.10(36) $\times 10^{-26}$ (TW)
	4724.1	6.30(16) $\times 10^{-24}$ (TW) ^a	4.44(43) $\times 10^{-26}$ (TW)
	4999.0	7.76(39) $\times 10^{-24}$ [16]	8.3(18) $\times 10^{-26}$ (TW)
	5121-5136 (10 pts)	3.70(20) $\times 10^{-23}$ -4.80(20) $\times 10^{-23}$ (TW)	
6300 cm^{-1} (1.6 μm)	5702-6854 (30 pts)	2.3 $\times 10^{-25}$ -1.9 $\times 10^{-23}$ (TW) ^b	

149

150 *Notes*

151 ^a A previous determination ($5.9(3)\times 10^{-24} \text{ cm}^2 \text{ molecule}^{-1} \text{ atm}^{-1}$) was obtained by OFCEAS in [29].

152 ^b Previous CRDS measurements in the 5875-6665 cm^{-1} range (10 pts) were reported in [18,19].
 153

154 2. Experimental setups and data acquisition

155 2.1 The CRDS spectrometers

156 Three cavity ring down spectrometers were used in this work. The 2.3 μm setup has been
 157 described in details in [21,30] while readers are referred to [31] for the two setups used in the
 158 1.6 μm region. Briefly, a distributed feedback (DFB) laser diode (either from Eblana
 159 Photonics or NEL) is coupled into a high finesse cavity composed of two mirrors with highly
 160 reflective coatings. The different measurement points in the 2.3 μm window (near 4435, 4522,
 161 4724, 4999 and 5130 cm^{-1}) are listed in **Table 1**. The set of DFB laser diodes at disposal
 162 allows for a continuous coverage of the 1.6 μm window. Thirty spectral points were selected
 163 to sample the 5702-6854 cm^{-1} spectral range. Each spectrometer employed mirrors (from
 164 Layertec) with coatings optimized for each of the spectral range of interest. Resonance
 165 between the laser emitted frequency, measured with a wavelength meter (model 621-A IR
 166 from Bristol), and a longitudinal mode of the optical cavity is achieved by dithering the cavity
 167 length with the output mirror mounted on a piezoelectric transducer. After filling of the cavity
 168 with photons at resonance, the injection of laser light is stopped thanks to an acousto-optic
 169 modulator and the purely exponential decay time of photons leaking from the cavity (i.e. the
 170 ring down (RD) time, τ) is measured with a photodiode. The absorption coefficient of the

171 absorbing gas, $\alpha(\nu)$, is then derived from the fitted RD time, at the laser frequency ν , with the
172 following equation:

$$173 \quad \alpha(\nu) = \frac{1}{c\tau(\nu)} - \frac{1}{c\tau_0(\nu)} \quad (1)$$

174 With c the speed of light and τ_0 the ring down time with the optical cavity empty or filled
175 with a non-absorbing gas.

176 Depending on the spectral region, the minimal detectable absorption coefficient of our
177 recorded spectra, α_{min} , varies from $5 \times 10^{-11} \text{ cm}^{-1}$ to a few 10^{-10} cm^{-1} . Pressures were measured
178 either with a 50 mbar or a 1000 mbar pressure gauge (ATM.1ST from STS, accuracy of
179 $\pm 0.1\%$ of the full scale). The temperature of the CRDS cell was continuously measured by a
180 temperature sensor (TSic 501 from IST, $\pm 0.1 \text{ K}$ accuracy) fixed on the external wall of the
181 cavity enveloped by thermal insulation foam.

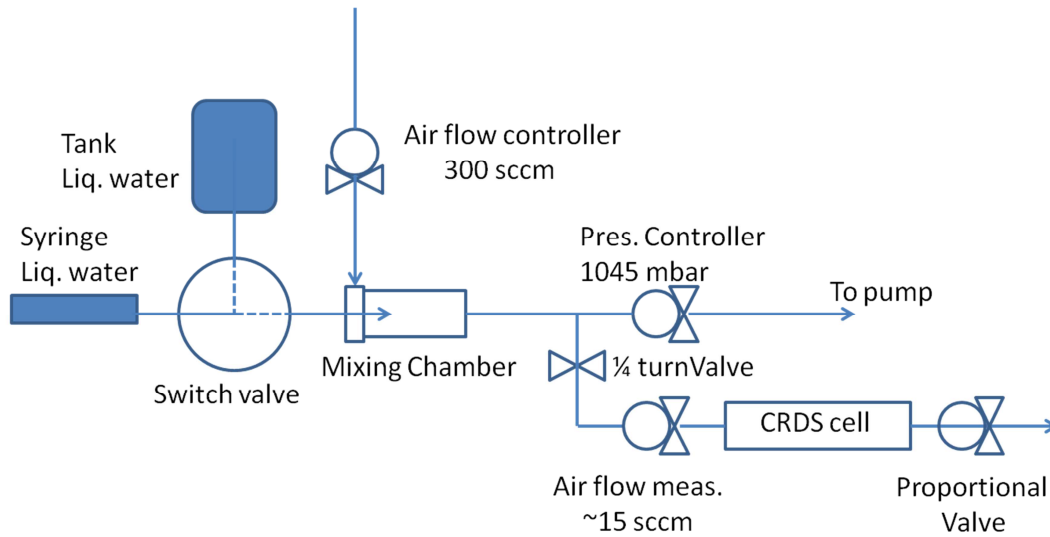
182 *2.2 Self-continuum data acquisition*

183 At the beginning of each day of measurements, the water sample was purified by cooling with
184 liquid nitrogen and pumping on the residual vapour phase. To determine the self-continuum
185 cross-sections, C_S , the absorption coefficient at a selected spectral point was recorded during
186 pressure ramps from 0 to 15 Torr (i.e. about 71% of the saturation pressure at 296 K). The
187 only exception was for measurements near 5130 cm^{-1} where the water monomer contribution
188 is particularly strong. Two spectra recorded in flow regime at 6 and 10 Torr were preferred to
189 the spectral ramp at fixed frequency in order to better account for the water monomer
190 contribution (see details below).

191 *2.3 Foreign-continuum data acquisition*

192 The measurements of the foreign-continuum absorption are more demanding as they require
193 to vary either the water vapour partial pressure of a moist air sample at fixed high pressure (a
194 few hundred Torr) or to vary the total pressure for a given water partial pressure by adding
195 dry air to the CRDS sample. This last method used in [21] is made difficult by the possible
196 modification of the optical alignment of the CRDS setup due to the large pressure changes. In
197 order to overcome this difficulty, we preferred the first method and recorded CRDS spectra
198 for different water vapour partial pressures (determined from absorption lines as detailed in
199 section 4.1), while maintaining the total pressure constant in the high finesse cavity. A
200 purpose-built humidifier was developed and a flow of humidified air was injected into the
201 CRDS cell for different controlled water vapour partial pressures up to about 6 Torr. The total
202 pressure was regulated at 700 Torr, for most of the measurements, with a downstream
203 proportional electrovalve controlled by a proportional-integral loop.

204 To vary the water vapour partial pressure in the dry air (Alphagaz 2 from Air Liquide), a
 205 syringe injection system, as described in details in [32], was used (**Fig. 1**). In this system a
 206 water droplet formed at the end of the syringe needle evaporates continuously in the
 207 surrounding air flow of the mixing chamber. The evaporation rate is proportional to the
 208 surface area of the droplet in contact with air. When this evaporation rate equals to liquid
 209 water supply rate, a steady-state is reached. The partial pressure of water vapour depends also
 210 of the dry air flow which is regulated together with the total pressure. A small part of the
 211 humidified air is derived into the CRDS cell where the total pressure is regulated with a
 212 proportional valve.



213

214

Figure 1. Scheme of the air humidifier based on a syringe injection system.

215 Depending on the liquid water injection rate and dry air flow, partial pressure of water vapour
 216 can be varied from 0 to 5.9 Torr in 700 Torr of air. This corresponds to a maximum relative
 217 humidity (RH) of 28% at 296 K. During the test phase, stabilities better than 0.3% were
 218 achieved over several tens of minutes for H₂O partial pressure up to 3.5 Torr (17% RH at 296
 219 K). Up to 6 Torr the system provides H₂O partial pressure with stability better than the
 220 percent level. At higher pressure the system becomes less stable and no measurements were
 221 realized.

222

3. Self-continuum

223

In a mixture of water vapor in air, the total absorption coefficient can be expressed as the sum
 224 of four terms:

225

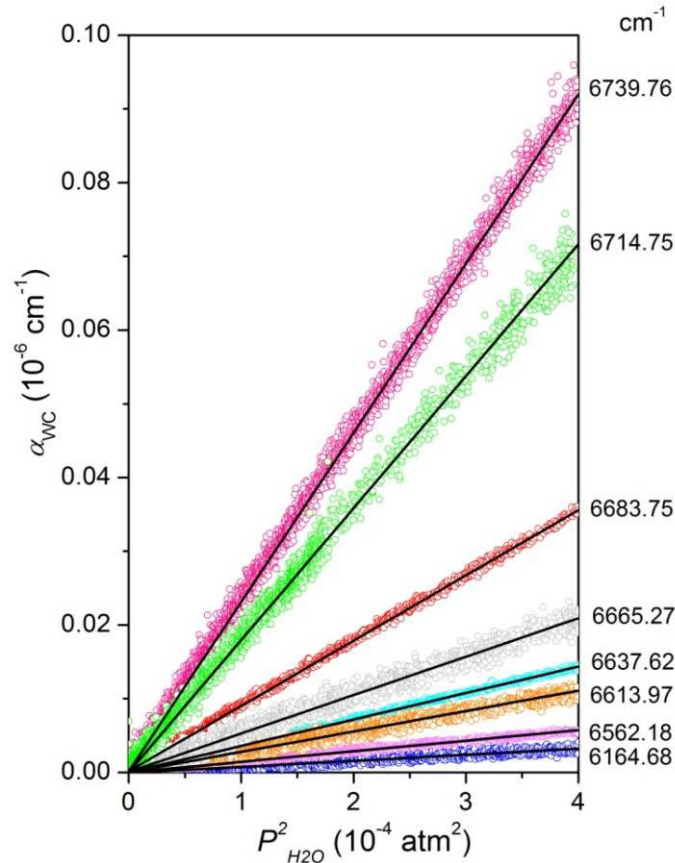
$$\alpha_{tot}(\nu, T) = \alpha_{cavity} + \alpha_{WML} + \alpha_{WCS} + \alpha_{WCF}$$

226

$$= \alpha_{cavity} + \alpha_{WML} + \frac{1}{kT} C_S(\nu, T) P_{H_2O}^2 + \frac{1}{kT} C_F(\nu, T) P_{H_2O} P_{air} \quad (2)$$

227 where α_{cavity} , α_{WML} , α_{WCS} and α_{WCF} are the contributions due to the cavity, water vapor
 228 “monomer local lines” (WML), water vapor self-continuum (WCS) and foreign-continuum
 229 (WCF). C_S and C_F cross-sections are expressed in $\text{cm}^2\text{molecule}^{-1}\text{atm}^{-1}$. Note that the
 230 negligible contribution of the Rayleigh scattering is omitted in Eq. (2).

231 *3.1. Self-continuum cross-sections retrieval*



232
 233 *Figure 2. Self-continuum absorption versus the squared water vapor pressure during pressure ramps*
 234 *up to 15 Torr for different spectral points of the 1.6 μm window. The self-continuum cross-section*
 235 *values were derived from the linear fits (black lines).*

236 The data treatment of the pressure ramps is the same as described in our previous papers
 237 [14,15,16]. A simulation of the water vapor rovibrational spectrum, α_{WML} , was performed at
 238 different pressures on the basis of the HITRAN2016 line list [33], using a Voigt profile and
 239 the standard $[-25, +25 \text{ cm}^{-1}]$ convention cut off for the line wings. For each spectral point, the
 240 quantity $(\alpha_{tot} - \alpha_{WML}) = (\alpha_{cavity} + \frac{1}{kT} C_S(\nu, T) P_{H_2O}^2)$ was plotted *versus* $P_{H_2O}^2$ and fitted by a linear
 241 function. The constant term corresponds to the absorption losses of the empty cavity, α_{cavity} ,
 242 while the self-continuum cross-section is obtained from the fitted value of the linear
 243 coefficient in $P_{H_2O}^2$. **Fig. 2** illustrates the pure quadratic dependence achieved in the present

244 recordings in the 1.6 μm window and the variation of the cross section *versus* the
 245 wavenumber. The C_S values derived in this way are listed in **Table 2** and presented in **Fig. 3**.
 246 In the last column of **Table 2**, the monomer relative contribution to the total absorption,
 247 $\alpha_{WML}/(\alpha_{WML} + \alpha_{WC})$, is given at each spectra point. Obviously, the spectral points were chosen
 248 in order to minimize as much as possible the contribution of rovibrational lines. Overall, the
 249 monomer contribution represents less than 12 % for the spectral points below 6300 cm^{-1} and
 250 then increases up to 70 % on the high energy edge of the window.

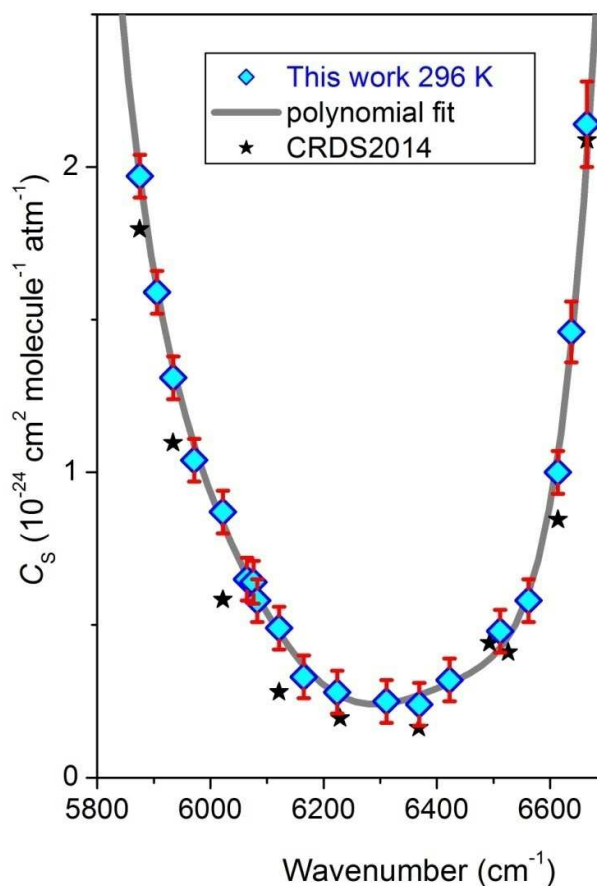
251 *Table 2. Self-continuum cross-sections in the 1.6 and 2.3 μm windows and corresponding relative*
 252 *contribution of the “local line monomer” to the total absorption. During the whole period of*
 253 *measurements temperature varied between 296 K and 298.5 K.*
 254

ν cm^{-1}	C_S $\text{cm}^2 \text{ molecule}^{-1} \text{ atm}^{-1}$	$\alpha_{WML}/(\alpha_{WML} + \alpha_{WC})$ %
2.3 μm window		
4724.07	$6.30(16) \times 10^{-24}$	4.0
5120.00	$3.7(20) \times 10^{-23}$	<i>a</i>
5135.00	$4.8(20) \times 10^{-23}$	<i>a</i>
1.6 μm window		
5702.13	$5.83(13) \times 10^{-24}$	11.91
5752.04	$4.43(6) \times 10^{-24}$	10.07
5780.40	$3.66(7) \times 10^{-24}$	6.57
5816.58	$3.04(7) \times 10^{-24}$	3.53
5842.21	$2.68(7) \times 10^{-24}$	3.70
5875.22	$1.97(7) \times 10^{-24}$	3.65
5905.72	$1.59(7) \times 10^{-24}$	2.72
5934.64	$1.31(7) \times 10^{-24}$	2.07
5971.09	$1.04(7) \times 10^{-24}$	5.33
6022.06	$8.7(7) \times 10^{-25}$	3.09
6064.57	$6.5(7) \times 10^{-25}$	6.08
6076.35	$6.4(7) \times 10^{-25}$	15.28
6082.69	$5.8(7) \times 10^{-25}$	1.18
6121.24	$4.9(7) \times 10^{-25}$	1.95
6164.68	$3.3(7) \times 10^{-25}$	1.44
6224.09	$2.8(7) \times 10^{-25}$	2.53
6311.03	$2.5(7) \times 10^{-25}$	12.87
6368.98	$2.4(7) \times 10^{-25}$	18.72
6422.57	$3.2(7) \times 10^{-25}$	19.82
6511.97	$4.8(7) \times 10^{-25}$	38.77
6562.18	$5.8(7) \times 10^{-25}$	32.85
6613.97	$1.00(7) \times 10^{-24}$	40.56
6637.62	$1.46(10) \times 10^{-24}$	39.78
6665.27	$2.14(14) \times 10^{-24}$	39.49
6683.95	$3.59(96) \times 10^{-24}$	72.08
6714.74	$7.3(10) \times 10^{-24}$	66.33
6739.76	$9.30(96) \times 10^{-24}$	57.07
6762.79	$1.56(17) \times 10^{-23}$	58.11
6808.32	$1.59(17) \times 10^{-23}$	62.63
6854.65	$1.87(10) \times 10^{-23}$	42.26

255

256 *Note*

257 ^a The listed C_S values were derived from the frequency dependence of C_S values at various measurement points in
 258 the 5121-5138 cm^{-1} interval. Depending of the selected spectral point, the monomer contribution represents
 259 between 39 and 92 % of the total absorption (see Text and insert in Fig. 4).



260

261 *Figure 3. Overview of the self-continuum cross-sections, C_S , in the 1.6 μm window. Black stars show*
 262 *the CRDS values of Ref. [19]. The grey curve corresponds to a 6th order polynomial fit of the present*
 263 *measurements (blue diamonds) in the 5800-6700 cm^{-1} interval: $C(v) = \sum_{i=0}^5 a_i v^i$ with a_i coefficient*
 264 *values of 2.69348×10^{-17} , -2.60041×10^{-20} , 1.04584×10^{-23} , -2.24283×10^{-27} , 2.70491×10^{-31} , -*
 265 *1.73944×10^{-35} and 4.65967×10^{-40} .*

266 In the 2.3 μm window, self-continuum measurements were performed near 4720 cm^{-1} and in
 267 the 5121-5136 cm^{-1} interval. C_S at 4720 cm^{-1} was already determined by OFCEAS in [29]
 268 with a set of mirrors giving ring down times limited to 14 μs . The set of mirrors of our CRDS
 269 spectrometer provides ring down times of about 150 μs at 4720 cm^{-1} which should allow
 270 improving the sensitivity of the OFCEAS recordings. This is the reason why we decided to
 271 repeat the C_S measurement at this spectral point. The C_S derivation at 4720 cm^{-1} was based on
 272 pressure ramp recordings up to 15 Torr as in the 1.6 μm window. Similar quality of the
 273 pressure squared dependence was obtained. The derived C_S value $(6.3(2) \times 10^{-24} \text{ cm}^2 \text{ molecule}^{-1}$
 274 $\text{atm}^{-1})$ is consistent with the OFCEAS value of Ref. [29] $(5.9(3) \times 10^{-24} \text{ cm}^2 \text{ molecule}^{-1} \text{ atm}^{-1})$.

275 A different experimental procedure was adopted for the C_S determinations around 5130 cm^{-1} .
276 Two spectra at 10 Torr and one spectrum at 6 Torr were recorded over the $5121\text{-}5136\text{ cm}^{-1}$
277 interval accessible with the laser diode at disposal. Our choice to use a series of spectra
278 instead of pressure ramps was motivated by the strong contribution of the monomer lines over
279 the considered region. Indeed, in this situation, the uncertainty on the intensities of the strong
280 lines located in the region (extended by $\pm 25\text{ cm}^{-1}$) may have a strong impact on the derived
281 foreign-continuum value. The recorded spectra were first corrected from the baseline
282 retrieved from spectra recorded with the CRDS cell evacuated. Then the monomer
283 contribution, simulated using the HITRAN2016 database, was subtracted. From the obtained
284 residuals, eleven spectral points were selected in micro-windows between absorption lines.
285 These points were chosen because we estimated that locally the monomer contribution
286 (ranging between 39 and 92%) was satisfactorily accounted for by the HITRAN simulation.
287 For each spectral point, the C_S values were derived from the remaining absorption ($\alpha_{tot} - \alpha_{WML} -$
288 α_{cavity}) due to self-continuum (Eq. 2). As detailed below (§3.4), the set of about 30 C_S values
289 was fitted by a linear function of the wavenumber. The recommended values at 5120 and
290 5135 cm^{-1} are included in **Table 2**.

291 *3.3. Error budget*

292 The stability of the spectrum baseline was checked over several hours from spectra recorded
293 successively and found to be better than $2\text{-}5 \times 10^{-10}\text{ cm}^{-1}$ i.e. at a level much below the level of
294 the continuum absorption. In addition, the coincidence of the measured continuum absorption
295 during increasing and decreasing pressure ramps together with the pure pressure squared
296 dependence clearly indicate that the baseline instability during pressure ramps has a marginal
297 contribution to the error budget. The error due to the measurement of the pressure is less than
298 0.04 Torr for the 50 mbar full range pressure gauge used for the self-continuum measurements
299 and is thus also negligible.

300 For C_S values derived from pressure ramps, the statistical error bars of the above pressure fits
301 range between 0.03 and 2.3% .

302 For a large part of the spectral points, the main source of uncertainty comes from the
303 subtracted monomer contribution. This is especially true for the high energy edge of the 1.6
304 μm window and the 5130 cm^{-1} point where the monomer contribution represents between
305 20% and 72% of the total absorption above 6368 cm^{-1} and up to 92% of the total absorption
306 around 5130 cm^{-1} (**Table 2**). Following the method proposed in Ref. [34], we estimated the
307 uncertainty due to the monomer lines by propagation of the uncertainties provided by
308 HITRAN2016 for the different spectroscopic parameters of the water vapour lines. In

309 practice, only the uncertainties on the line intensities and on the self-broadening coefficients,
 310 γ_{self} , have to be considered. We performed two simulations, one with all line intensities
 311 increased by their respective error bar which led to a $\delta\alpha_{int}(\nu)$ deviation from the usual
 312 HITRAN simulation and one with all γ_{self} coefficients increased by their error bar which led to
 313 a $\delta\alpha_{\gamma_{self}}(\nu)$ deviation. The uncertainty on α_{WML} was obtained from: $\delta\alpha_{WML}(\nu) =$
 314 $\left[\delta\alpha_{int}(\nu)^2 + \delta\alpha_{\gamma_{self}}(\nu)^2\right]^{1/2}$ and is the dominant contribution to the error budget when the
 315 monomer contribution is important. At the opposite, in the centre of the 1.6 μm window, α_{WML}
 316 represents no more than a few % and can be mostly neglected. In this case, a good indication
 317 about the error bar can be obtained from the dispersion of the experimental values. We have
 318 included in **Fig. 3**, the curve obtained from a 6th order polynomial fit of the measurements
 319 between 5800 and 6700 cm^{-1} . The *rms* of the residuals is about $7 \times 10^{-26} \text{ cm}^2 \text{ molecule}^{-1} \text{ atm}^{-1}$
 320 *i.e.* about 25 % of the C_s value at the centre of the window. The error bars included in **Table 2**
 321 correspond to the largest value between $\delta\alpha_{WML}(\nu)$ and $7 \times 10^{-26} \text{ cm}^2 \text{ molecule}^{-1} \text{ atm}^{-1}$ and are
 322 believed to be conservative.

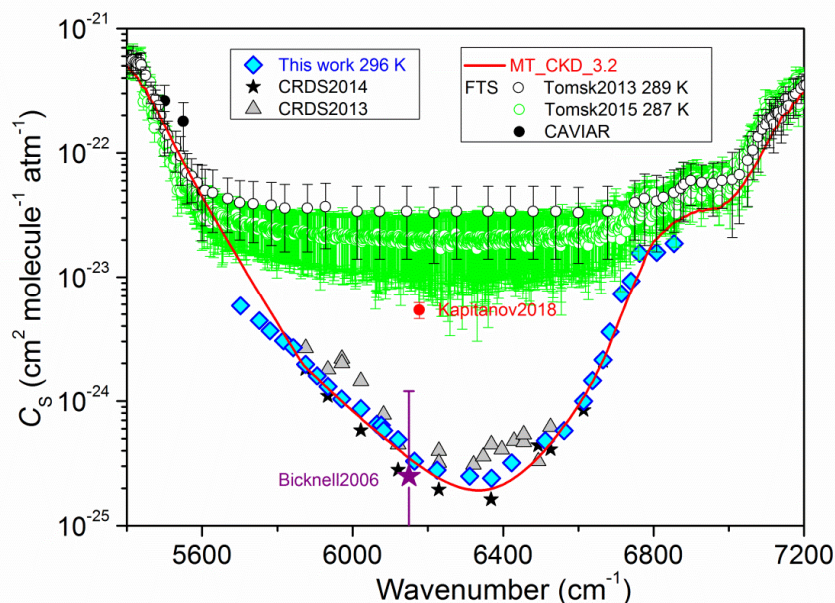
323 3.4. Comparison to literature values

324 The retrieved C_s values in the 1.6 μm window listed in **Table 2** are plotted in logarithmic
 325 scale in **Fig. 4** together with the most relevant literature data, in particular the two series of
 326 measurements performed by FTS in Tomsk [11, 12]. The present measurements in the 5702-
 327 6854 cm^{-1} range extend to the low- and high-energy edges of the window our previous CRDS
 328 datasets in the 5875-6665 cm^{-1} interval [18,19]. As mentioned above, in these previous works,
 329 the pressure dependence of the absorption continuum was found to include a linear pressure
 330 dependence. This linear contribution was relatively important in the centre of the window (see
 331 for example Fig. 4 of [18]) and prevented us to estimate properly the uncertainty on the C_s
 332 values derived from the quadratic term. The overall agreement with the present recordings is
 333 satisfactory. Compared to Ref. [19], maximum deviations of about a factor of 2 are noted at
 334 6022 and 6121 cm^{-1} . This is significantly above the combined error bars but the uncertainties
 335 in Ref. [19] were specified to exclude possible biases due to the adsorbate.

336 The higher quality of the present results performed with a new set of high reflective mirrors is
 337 illustrated by the purely quadratic pressure dependence obtained for all the measurement
 338 points (**Fig. 2**) and the reduced dispersion of the retrieved C_s values (**Fig. 3**). The present
 339 results take thus precedence over the older ones.

340 The strong overestimation of the data retrieved from FTS spectra at room temperature in the
 341 centre of the 2.1 μm [10,11,12] and 1.6 μm windows [11,12] has been discussed in details in

342 our previous contributions (see for example Ref. [14]). To our opinion, the FTS sensitivity
 343 and baseline stability of the FTS setups used are not sufficient for such measurements of weak
 344 continua. As a rule, reported C_S values should be systematically supported by a solid study of
 345 the pressure dependence of the absorption signal. For example no pressure dependence was
 346 reported in the FTS room temperature studies of Refs. [10,11,12].

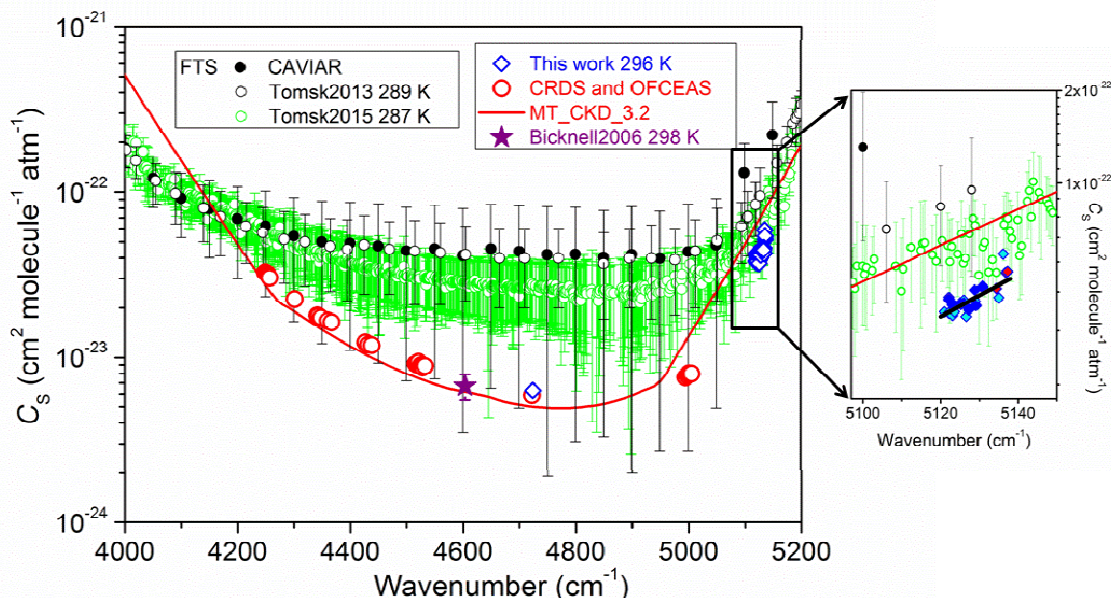


347
 348 *Figure 4. Overview of the self-continuum cross-sections, C_S , reported in the literature and retrieved in*
 349 *this work (blue diamonds) in the 1.6 μm window and comparison to the MT_CKD_3.2 continuum.*
 350 *Literature values were obtained by FTS in Ref. [11] (Tomsk2013), Ref. [12] (Tomsk2015) and Ref.*
 351 *[10] (CAVIAR), by photoacoustic spectroscopy in Ref. [35]), by interferometric calorimetry in Ref.*
 352 *[36](pink star) and by CRDS in Ref. [18](grey triangles) and Ref. [19] (black stars)*

353 A photoacoustic measurement was very recently reported by Kapitanov et al. [35] for the
 354 room temperature self-continuum at 6177 cm^{-1} . The reported C_S value ($5.4\pm 0.8\times 10^{-24}\text{ cm}^2$
 355 $\text{molecule}^{-1}\text{ atm}^{-1}$) included in **Fig. 4**, is intermediate between the FTS and CRDS values. For
 356 completeness, the value at 6150 cm^{-1} reported by Bicknell et al. by calorimetric interferometry
 357 [36] is added. Bicknell et al. performed only measurements for water vapor in N_2 at a total
 358 pressure of 770 Torr. The plotted C_S value at 6150 cm^{-1} is derived from the total continuum
 359 absorption of $3.2\pm 0.3\times 10^{-8}\text{ cm}^{-1}$ measured in [36] after subtraction of the foreign-continuum
 360 contribution. The latter is obtained from the CAVIAR foreign cross-section measured at 400
 361 K in [22] ($C_F= 3.2\pm 2.8\times 10^{-26}\text{ cm}^2\text{ molecule}^{-1}\text{ atmosphere}^{-1}$) assuming no temperature
 362 dependence. No water vapour partial pressure was given in [36] but a value of 25 Torr was
 363 estimated in [11]. As a result, the foreign-continuum is calculated to contribute to about 75 %

364 of the absorption measured by Bicknell. The propagation of the large uncertainty on the used
 365 C_F value leads to an uncertainty on C_S larger than its absolute value. Fortunately, the derived
 366 self-continuum cross-section ($2.5 \times 10^{-25} \text{ cm}^2 \text{ molecule}^{-1} \text{ atm}^{-1}$) is consistent with our
 367 measurements (see **Fig. 4**).

368 The overall agreement with the MT_CKD_3.2 semi-empirical cross-sections model is very
 369 good. This is not surprising as the MT_CKD_3.2 continuum was adjusted according to our
 370 previous CRDS results obtained below 6600 cm^{-1} [19]. We note that the agreement extends to
 371 the new measurement points above this wavenumber. Important differences (up to a factor
 372 2.3) are nevertheless observed on the newly measured low energy edge around 5700 cm^{-1} .
 373 The experimental results indicate that the MT_CKD continuum should be significantly
 374 reduced in this region



375
 376 *Figure 5. Overview of the experimental self-continuum cross-sections, C_S , reported in the literature*
 377 *and retrieved in this work (blue diamonds) for the $2.3 \mu\text{m}$ window and comparison to the*
 378 *MT_CKD_3.2 continuum. Literature values include FTS values from Ref. [11] (Tomsk2013), Ref. [12]*
 379 *(Tomsk2015) and CAVIAR [10]. The C_S value at 4605 cm^{-1} (purple star) was derived from the*
 380 *measurement of Bicknell et al. by interferometric calorimetry of a water vapour+ N_2 mixture [36]; the*
 381 *plotted value is corrected from the foreign-contribution (see Text). Open red circles correspond to the*
 382 *OFCEAS and CRDS values of Ref. [29] and Refs [14,15,16,21], respectively.*
 383 *In the insert, the series of measurements performed from three spectra near 5130 cm^{-1} are highlighted*
 384 *with diamonds filled with different colors. The recommended values correspond to the black solid line*
 385 *obtained from a fit of the measurement points.*

386 The new C_S values between 5120 and 5137 cm^{-1} concern the high energy edge of the $2.3 \mu\text{m}$
 387 window where CRDS measurements were missing. As mentioned above, they were obtained

388 from a series of three spectra recorded at 6 and 10 Torr and extend over the 5121-5138 cm^{-1}
389 interval. The different series of measurement points, highlighted in the insert of **Fig. 5**, show a
390 clear increase with the wavenumber values. The set of about 30 C_S values was fitted by a
391 linear function of the wavenumber. The corresponding fitted values at 5120 and 5135 cm^{-1} are
392 given in **Table 2**. Taking into account the statistical averaging of the error bars which are
393 mostly due to the uncertainties on the water monomer, we estimate to $\sim 2 \times 10^{-23} \text{ cm}^2 \text{ molecule}^{-1}$
394 atm^{-1} the resulting error bars which represents 54% and 42% of the C_S value at 5120 cm^{-1} and
395 5135 cm^{-1} , respectively. Note that only 2% dispersion is observed around the linear function
396 fitted to the ~ 30 C_S values in the 5121-5138 cm^{-1} interval which might indicate that the
397 estimated error bar are overestimated.

398 The present and previous CRDS and OFCEAS data in the 2.3 μm window [14,15,16,21,29]
399 are plotted in **Fig. 5** together with FTS data from Refs. [10,11,12]. Similarly to the 1.6 μm
400 window, the current 3.2 version of the MT_CKD continuum was adjusted to our previous
401 measurements below 4800 cm^{-1} [14,15,16,21,29]. Near 5130 cm^{-1} , the present results are
402 found to be about a factor 1.5 smaller than MT_CKD_3.2 values. The agreement with the
403 FTS values, in particular with Tomsk2015 [12], is significantly better than for the other
404 CRDS spectral points of the window. This agreement results from the strong value of C_S at
405 5130 cm^{-1} (about $4 \times 10^{-23} \text{ cm}^2 \text{ molecule}^{-1} \text{ atm}^{-1}$) which is close to the mostly constant FTS
406 values reported near room temperature between 4400 and 5000 cm^{-1} [10,11,12] and between
407 5700 and 6700 cm^{-1} [11,12] and that can be considered as the detectivity threshold of the
408 CAVIAR and Tomsk setups.

409 We have also considered the room temperature measurement reported by Bicknell et al. by
410 calorimetric interferometry near 4605 cm^{-1} for a mixture of 14.7 Torr of water vapour in N_2 at
411 a total pressure of 770 Torr [36]. The calculated monomer contribution ($7 \times 10^{-9} \text{ cm}^{-1}$) was
412 subtracted from the total absorption ($1.0 \times 10^{-7} \text{ cm}^{-1}$) obtained from Fig. 8 of Ref. [36]. The
413 foreign-contribution in the conditions of Ref. [36] was determined using the C_F value
414 ($6.7 \times 10^{-26} \text{ cm}^2 \text{ molecule}^{-1} \text{ atm}^{-1}$) interpolated from our C_F determinations at 4522.0 and 4724.1
415 cm^{-1} (see below and **Table 1**). As a result, we obtain a C_S value of $6.7 \times 10^{-24} \text{ cm}^2 \text{ molecule}^{-1}$
416 atm^{-1} , included in **Fig. 5**, which shows a very good consistency with our results.

417

418

4 Foreign-continuum

419

4.1. Cross-section retrieval

420

421

422

423

424

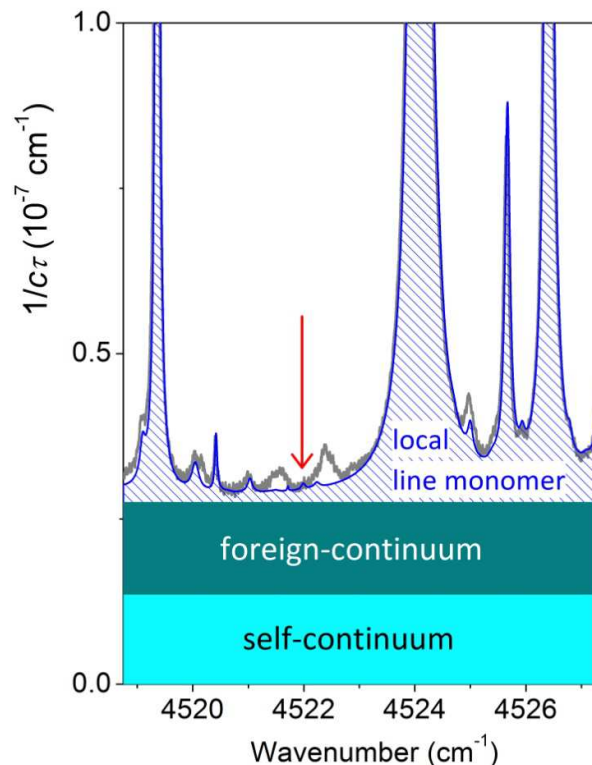
425

426

427

428

As mentioned above the foreign-continuum measurements were performed on the basis of spectra recorded over a few cm^{-1} around 4435, 4522, 4720 and 4999 cm^{-1} . The recordings were performed in flow regime with constant total pressure (generally 700 Torr) and different partial pressures of water vapour up to 6 Torr. For each water concentration, two successive spectra were recorded to check the concentration stability. All the spectra were first corrected from the background spectrum obtained with dry air at the same total pressure to ensure no change in the mirror alignment. As very small losses due to Rayleigh scattering are mostly identical in this background and in the moist air spectra, the Rayleigh contribution was omitted in Eq. (2).



429

430

431

432

433

434

435

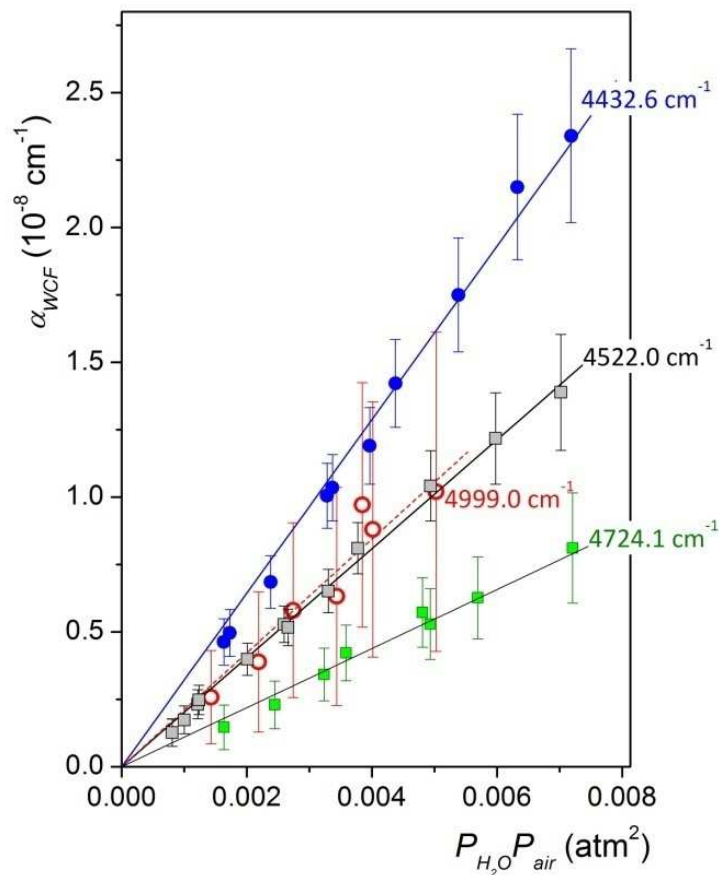
436

437

Figure 6. Part of the spectrum recorded around 4522 cm^{-1} for a mixture of water vapour in air (5.85 Torr of H_2O in 693.35 Torr of air) and corrected from the background spectrum recorded with dry air at the same total pressure. The “local line monomer”, self-continuum and foreign-continuum contributions are indicated. The red arrow shows one of the selected measurement points.

For each recorded spectrum, the water vapour partial pressure, $P_{\text{H}_2\text{O}}$, was determined from a line profile fit of a few isolated water lines. Water lines with low uncertainty intensity values were taken from the HITRAN2016 database. The water monomer contribution was then

438 simulated for the experimental conditions of the recordings - P_{H_2O} , P_{tot} , T - using the
 439 HITRAN2016 database and the usual $[-25 \text{ cm}^{-1}, +25 \text{ cm}^{-1}]$ line profile cut-off. This α_{WML}
 440 contribution was then subtracted from $(\alpha_{tot} - \alpha_{cavity})$ together with the absorption contribution of
 441 the self-continuum, α_{WCF} . The latter was calculated using the self-continuum cross-section
 442 values determined in our previous works and the value at 4720 cm^{-1} updated in this work (see
 443 **Table 1**). **Figure 6** shows the different contributions to the absorption continuum near 4520
 444 cm^{-1} . For a partial pressure of water vapour of about 6 Torr in air at a total pressure of 700
 445 Torr, the self- and foreign-contributions have similar amplitude, the monomer lines
 446 contribution being smaller at this spectral point. The different foreign-continuum cross-
 447 section values given in **Table 1**, were retrieved from the fitted slope of $(\alpha_{tot} - \alpha_{cavity} - \alpha_{WML} -$
 448 $\alpha_{WCS})$ versus $P_{H_2O}P_{air}$ (see Eq. 2). **Fig. 7** shows the achieved linear dependence for four
 449 measurement points.



450

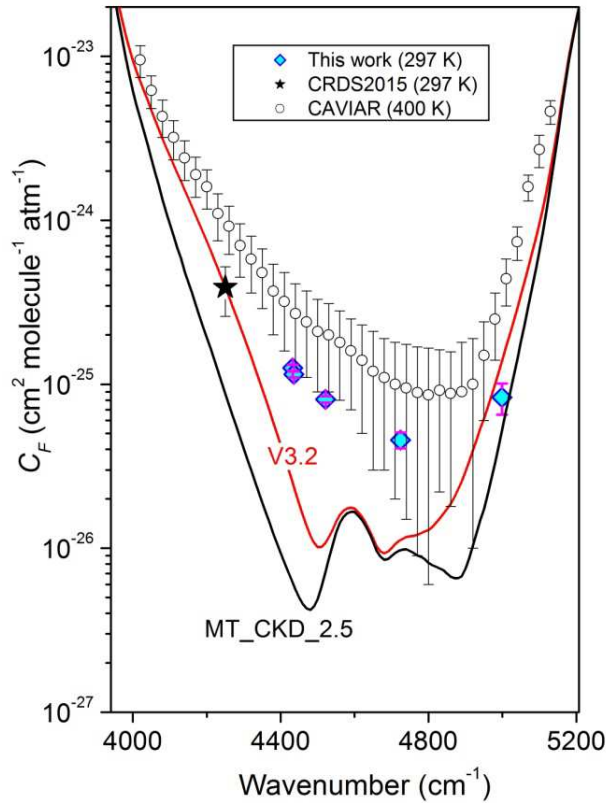
451 *Figure 7. Foreign-continuum absorptions at the selected spectral points and corresponding fitted*
 452 *slopes (solid lines).*

453
454
455
456
457
458
459
460
461
462
463
464
465
466
467
468
469
470
471
472
473
474
475
476
477
478
479
480
481

4.2. Comparison to literature values

The comparison of the available experimental determination of the foreign-continuum cross-sections in the 2.3 μm window to the MT_CKD_3.2 values is presented in **Fig. 8**. Experimental data at room temperature are limited to the present determinations around four spectral points and our previous CRDS data point at 4250 cm^{-1} [21]. The CAVIAR consortium reported foreign-continuum absorption by FTS between 1.1 and 5 μm at high temperatures (350-431 K) with an absorption path length of 17.7 m. The chosen elevated temperatures allow increasing the water vapour partial pressure of the recordings between 266 and 600 mbar. Compared to our measurement conditions (less than 6 Torr of water in air at about 1 atm), these high water vapour pressure values combined with air pressure of about 4 atm led to an increase of the foreign-continuum absorption signal by two or three orders of magnitude. The FTS recordings between 350 and 431 K did not reveal temperature dependence greater than the uncertainty in those measurements. The C_F values at the 400 K average temperature reported by Ptatshnik et al. [22] are plotted on **Fig. 8**. Note that the MT_CKD foreign-continuum also included in the figure is assumed to be temperature independent. Our room temperature C_F values are systematically below the FTS values (at 400 K) by a factor between 2 and 4. Although the FTS values were reported with very large error bars (between 30 and 93 %), the CRDS values fall outside the 1σ FTS confidence interval except at 4724 cm^{-1} . If these FTS values at 400 K are confirmed, it would indicate that the foreign-continuum exhibits small *positive* temperature dependence.

In the centre of the window, the CRDS dataset shows a disagreement of typically a factor 5 with the cross-sections given by the MT_CKD_3.2 model. The agreement is much better for the two measurement points on the low and high energy range of the window (at 4250 and 4999 cm^{-1} , respectively). In fact the MT_CKD foreign-continuum was recently significantly increased in the 2.3 μm window, taking into account our CRDS value at 4250 cm^{-1} [21] and the NIST values [27] (the MT_CKD_2.5 is included in **Fig. 8**, for comparison). The obtained CRDS results indicate that the MT_CKD foreign-continuum should be significantly increased in the centre of the window, too.



482

483 *Figure 8. Overview of the foreign-continuum cross-sections, C_F , reported in the literature and*
 484 *retrieved in this work for the 2.3 μm window and comparison to the MT_CKD model in its versions*
 485 *3.2 (red) and 2.5 (black). Previous experimental determinations are limited to the CAVIAR FTS values*
 486 *at 400 K from Ref. [22] (open black circles) and the CRDS value at 4250 cm^{-1} of Ref. [21].*

487 4.3. Error budget

488 Uncertainties on the derived C_F values have been calculated with the error propagation
 489 approach using Eq. 2 and assuming uncorrelated variables. In general, error bars on C_F are
 490 expected to be larger than those on C_S , as the foreign continuum is the residuals obtained after
 491 subtraction of the self-continuum and monomer contributions. From spectra recorded
 492 successively with the same amount of water vapour, the baseline stability was evaluated to be
 493 in the $5\text{-}8 \times 10^{-10} \text{ cm}^{-1}$ range, depending on the measurement point. Uncertainties on
 494 temperature and total pressure are deduced from the accuracies given by the temperature
 495 sensor and pressure gauges manufacturers and are mostly negligible. The C_S values and
 496 corresponding error bars were taken in our original paper (see **Table 1**), except near 4724
 497 cm^{-1} where we used the results obtained in this work.

498 The water vapour partial pressure is a major error source as it impacts both the self-continuum
 499 contribution proportional to $P_{\text{H}_2\text{O}}^2$ and the monomer contribution proportional to $P_{\text{H}_2\text{O}}$. As

500 mentioned above, this quantity was retrieved from the area of well-isolated H₂O lines fitted
501 with a Voigt profile using their HITRAN2016 intensity values. The relative uncertainty on
502 P_{H_2O} is mostly determined by the error bar on the intensity value, the uncertainty on the fitted
503 area being negligible. It leads to error bars on the order of 5% for all the measurement points
504 but the 4999.0 cm⁻¹ spectral point where a 10 % value was adopted.

505 The uncertainty due to the monomer contribution, α_{WML} , was calculated in the same way as
506 presented in Section 3.3 for the self-continuum. The error bars on the line intensities, self-
507 broadening and air-broadening coefficients were considered together with the uncertainty on
508 the water vapour pressure. Four simulations, $\delta_i(\nu)$, were performed, each of them with either,
509 the intensities, γ_{self} , γ_{air} coefficients or P_{H_2O} values increased by their error bar. The
510 uncertainty on α_{WML} was obtained from: $\delta\alpha_{WML}(\nu) = [\sum_{i=1}^4 \delta_i(\nu)^2]^{1/2}$.

511 Combining the different error sources, we obtained, for each spectral point, the error bar on
512 α_{WCF} for each P_{H_2O} value (see **Fig. 7**). The final C_F uncertainty included in **Table 1** was
513 calculated as the square root of the variance of the linear fit of the foreign absorption
514 coefficient *versus* $P_{H_2O}P_{air}$ as illustrated in **Fig. 7**. In this fit, each data point was weighted
515 according to its error bar, the weight being taken as the inverse of the squared uncertainty.

516 Finally, we considered the possible contribution of the N₂ collision induced absorption (CIA)
517 band near 4630 cm⁻¹ to the foreign-continuum measurements at 4720 cm⁻¹. This weak CIA
518 band corresponds to the 2-0 first overtone band of N₂. Experimentally, it was investigated at
519 room temperature [37] and at 97.5 K [38], a long time ago. Very recently, Hartmann et al.
520 performed classical molecular dynamic simulations (CMDS) of the 2-0 N₂ CIA [39] and
521 achieved a very satisfactory agreement with these pioneer experimental works. Note that, near
522 its maximum, the amplitude of the CIA absorption for N₂ at 1 atm is about 10⁻⁸ cm⁻¹, i.e. on
523 the same order of magnitude as the absorption due to the foreign-continuum of 5 Torr of
524 water vapour in 1 atm of air. The experimental procedure adopted in this work for the foreign-
525 continuum measurements excludes a possible bias due to the contribution of the N₂ 2-0 CIA.
526 Indeed, the baseline of the background spectrum recorded with dry air at 700 Torr includes
527 the N₂ CIA in air which is thus subtracted from the spectrum of moist air. A marginal
528 contribution of the CIA may nevertheless be possible due to the fact that for a given total
529 pressure, a few Torr of air in the background spectrum are replaced by water vapour. The
530 enhancement of the N₂ CIA by water vapour has been evidenced by Baranov [25] in the
531 region of the 1-0 fundamental band. Nevertheless, CMDS calculations indicate that for the 2-0

532 CIA, the enhancement is not sufficient to contribute significantly to the continuum in our low
533 pressure conditions.

534 **5. Conclusion**

535 In the present work, the accuracy of the self-continuum cross-sections of water vapor has been
536 improved by CRDS in the 1.6 μm window and at the 4720 cm^{-1} spectral point of the 2.3 μm
537 window. In addition, the spectral coverage of the 1.6 μm window was extended at low and
538 high energies and a new spectral point of the 2.3 μm window was measured at 5130 cm^{-1} . In
539 the context of the debate about the large discrepancies between FTS and laser-based
540 measurements at room temperature in the transparency windows [20], our first measurements
541 in the 1.6 μm were questioned because a non purely quadratic pressure squared dependence
542 was observed. In these earlier CRDS works, the sensitivity of the CRDS technique allowed
543 evidencing and measuring a small absorption signal proportional to the water vapor pressure
544 which was attributed to water adsorbed on the mirrors used at that time. This linear term
545 added some uncertainty to the derived C_S values. In the present recordings performed with a
546 better set of high reflective mirrors, a pure pressure squared dependence is obtained for all the
547 measurement points. Although showing a general agreement with the present more accurate
548 results, cross section values reported in Refs. [18,19] were partly affected by errors related to
549 adsorption.

550 As the 3.2 version of the MT_CKD model in the 2.3 and 1.6 μm windows was constrained
551 according to our previous measurements, the overall agreement is very good. The most
552 significant deviations concern newly measured spectral points in the low energy edge of the
553 1.6 μm window near 5700 cm^{-1} and in the high energy edge of the 2.3 μm window near 5130
554 cm^{-1} where measurements are lower than MT_CKD by about a factor of 2 and 1.5,
555 respectively.

556 In general, accurate measurements of the water vapor foreign-continuum are more demanding
557 as the C_F cross-sections are directly impacted by the uncertainty on the water vapor partial
558 pressure in moist air used for the measurements and by the uncertainties on the self-
559 continuum and on the water monomer contributions. In this work, C_F values were newly
560 determined with error bars ranging between 4 and 22 % at four spectral points of the 2.3 μm
561 window, between 4430 and 5000 cm^{-1} . The measurements are found consistent with the
562 previous CRDS measurement at 4250 cm^{-1} [21] which has led to an increase of the MT_CKD
563 foreign continuum at this spectral point. The new measurements confirm the underestimation

564 of the MT_CKD continuum in the centre of the 2.3 μm window where an increase by a factor
565 of 5 is suggested.

566

567 **Acknowledgments**

568 This project is supported by the Labex OSUG@2020 (ANR10 LABX56) and the LEFE-ChAt
569 program from CNRS-INSU. The authors want to thank J.-M. Hartmann (LMD) for providing
570 them classical molecular dynamic calculations of the N_2 CIA in a N_2 - H_2O mixture.

571 **References**

-
- [1] Cubasch U, Wuebbles D, Chen D, Facchini MC, Frame D, Mahowald N, Winther J-G, 2013: Introduction. In: *Climate Change 2013: The Physical Science Basis. Contribution of Working Group I to the Fifth Assessment Report of the Intergovernmental Panel on Climate Change* [Stocker, T.F., D. Qin, G.-K. Plattner, M. Tignor, S.K. Allen, J. Boschung, A. Nauels, Y. Xia, V. Bex and P.M. Midgley (eds.)]. Cambridge University Press, Cambridge, United Kingdom and New York, NY, USA.
- [2] Shine KP, Ptashnik IV, Rädcl G. The Water Vapour Continuum: Brief History and Recent Developments, *Surv Geophys* 2012;33:535–555. DOI:10.1007/s10712-011-9170-y.
- [3] Serov EA, Odintsova TA, Tretyakov MY, Semenov ME. On the origin of the water vapour continuum absorption within rotational and fundamental vibrational bands. *J Quant Spectrosc Radiat Transfer* 2017;193:1–12. DOI: 10.1016/j.jqsrt.2017.02.011
- [4] Clough SA, Kneizys FX, Davies RW. Line shape and the water vapor continuum. *Atmospheric Research* 1989;23:229-241. DOI:10.1016/0169-8095(89)90020-3.
- [5] Mlawer EJ, Payne VH, Moncet J, Delamere JS, Alvarado MJ, Tobin DC. Development and recent evaluation of the MT_CKD model of continuum absorption. *Phil Trans R Soc A* 2012;370:2520–2556. DOI:10.1098/rsta.2011.0295.
- [6] Burch DE. Continuum absorption by H_2O . Report AFGL-TR-81-0300, Air Force Geophys. Laboratory, Hanscom AFB, MA, 1982.
- [7] Burch DE, Alt RL. Continuum absorption by H_2O in the 700 – 1200 cm^{-1} and 2400 – 2800 cm^{-1} windows. Report AFGL-TR-84-0128, Air Force Geophys. Laboratory, Hanscom AFB, MA., 1984.
- [8] Burch DE. Absorption by H_2O in narrow windows between 3000 and 4200 cm^{-1} . Report AFGL-TR-85-0036, Air Force Geophys. Laboratory, Hanscom AFB, MA., 1985.
- [9] Paynter DJ, Ptashnik IV, Shine KP, Smith KM, McPheat R, Williams RG. Laboratory measurements of the water vapor continuum in the 1200–8000 cm^{-1} region between 293 K and 351 K. *J Geophys Res* 2009;114:D21301. DOI:10.1029/2008JD011355.
- [10] Ptashnik IV, McPheat RA, Shine KP, Smith KM, Williams RG. Water vapor self-continuum absorption in near-infrared windows derived from laboratory measurements. *J Geophys Res* 2011;116: D16305. DOI:10.1029/2011JD015603.
- [11] Ptashnik IV, Petrova TM, Ponomarev YN, Shine KP, Solodov AA, Solodov AM. Near-infrared water vapour self-continuum at close to room temperature. *J Quant Spectrosc Radiat Transfer* 2013;120:23–35. DOI:10.1016/j.jqsrt.2013.02.016.
- [12] Ptashnik IV, Petrova TM, Ponomarev YN, Solodov AA, Solodov AM. Water vapor continuum absorption in near-IR atmospheric windows. *Atmos Oceanic Opt* 2015;28:115–120. DOI:10.1134/S102485601502009.
- [13] Cormier JG, Ciurylo R, Drummond JR. Cavity ringdown spectroscopy measurements of the infrared water vapor continuum. *J Chem Phys* 2002;116:1030–1034. DOI:10.1063/1.1425825.
- [14] Campargue A, Kassi S, Mondelain D, Vasilchenko S, Romanini D. Accurate laboratory determination of the near infrared water vapor self-continuum: A test of the MT_CKD model. *J Geophys Res Atmos* 2016;121:13,180 – 13,203. DOI:10.1002/2016JD025531.

-
- [15] Richard L, Vasilchenko S, Mondelain D, Ventrillard I, Romanini D, Campargue A. Water vapor self-continuum absorption measurements in the 4.0 and 2.1 μm transparency windows. *J Quant Spectrosc Radiat Transf* 2017;201:171–179. DOI: 10.1016/j.jqsrt.2017.06.037.
- [16] Lechevallier L, Vasilchenko S, Grilli R, Mondelain D, Romanini D, Campargue A. The water vapour self-continuum absorption in the infrared atmospheric windows: new laser measurements near 3.3 and 2.0 μm . *Atmos Meas Tech* 2018;11:2159–2171. DOI:10.5194/amt-11-2159-2018.
- [17] http://rtweb.aer.com/continuum_description.html
- [18] Mondelain D, Aradj A, Kassi S, Campargue A. The water vapor self-continuum by CRDS at room temperature in the 1.6 μm transparency window. *J Quant Spectrosc Radiat Transfer* 2013;130:381–391. DOI:10.1016/j.jqsrt.2013.07.006.
- [19] Mondelain D, Manigand S, Kassi S, Campargue A. Temperature dependence of the water vapor self-continuum by cavity ring-down spectroscopy in the 1.6 μm transparency window. *J Geophys Res Atmos* 2014;119:2169–8996. DOI:10.1002/2013JD021319.
- [20] Shine KP, Campargue A, Mondelain D, McPheat RA, Ptashnik IV, Weidmann D. The water vapour continuum in near-infrared windows – current understanding and prospects for its inclusion in spectroscopic databases. *J Mol Spectrosc* 2016;327:193–208. DOI:10.1016/j.jms.2016.04.011.
- [21] Mondelain D, Vasilchenko S, Cermak P, Kassi S, Campargue A. The self- and foreign-absorption continua of water vapor by cavity ring-down spectroscopy near 2.35 μm . *Phys Chem Chem Phys* 2015;17:17762. DOI:10.1039/C5CP01238D.
- [22] Ptashnik IV, McPheat RA, Shine KP, Smith KM, Williams RG. Water vapour foreign-continuum absorption in near-infrared windows from laboratory measurements, *Phil Trans R Soc A* 2012;370:2557–2577. DOI:10.1098/rsta.2011.0218.
- [23] Hartmann J-M, Tran H, Armante R, Boulet C, Campargue A, Forget F, Gianfrani L, Gordon I, Guerlet S, Gustafsson M, Hodges JT, Kassi S, Lisak D, Thibault F, Toon GC. Recent advances in collisional effects on spectra of molecular gases and their practical consequences, *J Quant Spectrosc Radiat Transfer* 2018;213:178–227. DOI: 10.1016/j.jqsrt.2018.03.016.
- [24] Cormier JG, Hodges JT, Drummond JR. Infrared water vapor continuum absorption at atmospheric temperatures. *J Chem Phys* 2005;122:114309.
- [25] Baranov YI. The continuum absorption in $\text{H}_2\text{O}+\text{N}_2$ mixtures in the 2000–3250 cm^{-1} spectral region at temperatures from 326 to 363 K. *J Quant Spectrosc Radiat Transfer* 2011;112:2281–2286. DOI:10.1016/j.jqsrt.2011.06.005.
- [26] Baranov YI, Buryak IA, Lokshantov SE, Lukyanchenko VA, Viganin AA. $\text{H}_2\text{O}-\text{N}_2$ collision-induced absorption band intensity in the region of the N_2 fundamental: ab initio investigation of its temperature dependence and comparison with laboratory data. *Phil Trans R Soc A* 2012;370:2691–2709. DOI: 10.1098/rsta.2011.0189.
- [27] Baranov YI and Lafferty WJ. The water vapour self- and water-nitrogen continuum absorption in the 1000 and 2500 cm^{-1} atmospheric windows. *Phil Trans R Soc A* 2012;370:2578–2589. DOI: 10.1098/rsta.2011.0234
- [28] Brogniez H, English S, Mahfouf JF, Behrendt A, Berg W, Boukabara S, Buehler SA, Chambon P, Gambacorta A, Geer A, Ingram W, Kursinski ER, Matricardi M, Odintsova TA, Payne VH, Thorne PW, Tretyakov MY, Wang J. A review of sources of systematic errors and uncertainties in observations and simulations at 183 GHz. *Atmos Meas Tech* 2016;9:2207–2221. DOI:10.5194/amt-9-2207-2016.
- [29] Ventrillard I, Romanini D, Mondelain D, Campargue A. Accurate measurements and temperature dependence of the water vapor self-continuum absorption in the 2.1 μm atmospheric window. *J Chem Phys* 2015;143:134304. DOI:10.1063/1.4931811.
- [30] Mondelain D, Vasilchenko S, Čermák P, Kassi S, Campargue A. The CO_2 absorption spectrum in the 2.3 μm transparency window by high sensitivity CRDS: (II) Self-absorption continuum. *J Quant Spectrosc Radiat Transfer* 2017;187:38–43. DOI: 10.1016/j.jqsrt.2016.09.003.
- [31] Kassi S, Campargue A. Cavity ring down spectroscopy with $5 \times 10^{-13} \text{ cm}^{-1}$ sensitivity. *J Chem Phys* 2012;137:234201. DOI: 10.1063/1.4769974.
- [32] Landsberg, J 2014, Development of an OF-CEAS laser spectrometer for water vapor isotope measurements at low water concentrations, Doctor of Philosophy, University of Groningen, [S.I.].

-
- [33] Gordon IE, Rothman LS, Hill C, Kochanov RV, Tan Y, Bernath PF, Birk M, Boudon V, Campargue A, Chance KV, Drouin BJ, Flaud JM, Gamache RR, Hodges JT, Jacquemart D, Perevalov, VI, Perrin A, Shine KP, Smith MAH, Tennyson J, Toon GC, Tran H, Tyuterev VG, Barbe A, Császár, AG, Devi VM, Furtenbacher T, Harrison JJ, Hartmann J-M, Jolly A, Johnson TJ, Karman T, Kleiner, I, Kyuberis AA, Loos J, Lyulin OM, Massie ST, Mikhailenko SN, Moazzen-Ahmadi N, Müller HSP, Naumenko OV, Nikitin AV, Polyansky OL, Rey M, Rotger M, Sharpe SW, Sung K, Starikova E, Tashkun SA, Vander Auwera J, Wagner G, Wilzewski J, Wcisło P, Yu S, Zak EJ. The HITRAN2016 Molecular Spectroscopic Database. *J Quant Spectrosc Radiat Transf* 2017;203:3-69. DOI: 10.1016/j.jqsrt.2017.06.038.
- [34] Ptashnik IV. Evaluation of suitable spectral intervals for near-IR laboratory detection of water vapour continuum absorption. *J Quant Spectrosc Radiat Transfer* 2007;108:146–160. DOI:10.1016/j.jqsrt.2007.03.011.
- [35] Kapitanov VA, Osipov KY, Ptashnik IV. Photoacoustic measurements of the water vapor continuum absorption in the 1.6 μm window. *Optika Atmosfery i Okeana* 2018;31:995–1000 [in Russian].
- [36] Bicknell WE, Cecca SD, Griffin MK. Search for low-absorption regions in the 1.6- and 2.1- μm atmospheric windows. *J Directed Energy* 2006;2:151–61.
- [37] Shapiro MM, Gush HP. The collision-induced fundamental and first overtone bands of oxygen and nitrogen. *Can J Phys* 1966;44:949-963.
- [38] McKellar ARW. Low-temperature infrared absorption of gaseous N_2 and $\text{N}_2 + \text{H}_2$ in the 2.0–2.5 μm region: Application to the atmospheres of Titan and Triton. *Icarus* 1989;80:361–369.
- [39] Hartmann J-M, Boulet C, Toon GC. Collision-induced absorption by N_2 near 2.16 μm : Calculations, model, and consequences for atmospheric remote sensing. *J Geophys Res Atmos* 2017;122:2419–2428. DOI:10.1002/2016JD025677.

